# Wavelength Division Multiplexing in Long-Haul Transoceanic Transmission Systems

Neal S. Bergano, *Fellow, IEEE, Fellow, OSA*

*Invited Tutorial*

***Abstract*—Wavelength division multiplexing (WDM) technology used in long-haul transmission systems has steadily progressed over the past few years. Newly installed state-of-the-art transoceanic systems now have terabit per second maximum capacity, while being flexible enough to have an initial deployed capacity at a fraction of the maximum. The steady capacity growth of these long-haul fiber-optic cable systems has resulted from many improvements in WDM transmission techniques and an increased understanding of WDM optical propagation. Important strides have been made in areas of dispersion management, gain equalization, modulation formats, and error-correcting codes that have made possible the demonstration of capacities approaching 4 Tb/s over transoceanic distances in laboratory experiments.**

***Index Terms*—Long-haul telecommunications, optical amplifier, undersea optical communications, wavelength division multiplexing (WDM).**

## I. Introduction

IN TODAY'S Internet age, information flows across continents just as easy as it flows across the office [1]. With so many "point-and-click" virtual connections, it is easy to forget that the world's communications needs are made possible by real systems, based on fiber-optic cables [2]. This, of course, comes as no surprise to those of us in the telecommunications community; however, many others underestimate the importance of undersea fiber-optic cables for intercontinental telecommunications. Anyone who makes international phone calls, sends international faxes, or simply surfs the web at sites on other continents uses undersea fiber-optic cables. This global connectivity is evident from the world map displayed in Fig. 1, which shows the majority of installed undersea cables.

This paper will review some of the more important issues regarding the use of wavelength division multiplexing (WDM) in long-haul transmission systems. This work is written from the perspective of getting optical data from points "A to B" across a long optical link (i.e., link centric rather than network centric). Included will be an introduction to long-haul undersea transmission systems, the amplified transmission line, dispersion/nonlinear management, transmission formats, measures of system performance, forward error correction (FEC), experimental techniques, a transmission line design example, and future trends.

Manuscript received April 7, 2005; revised July 21, 2005.

The author is with Tyco Telecommunications, Eatontown, NJ 07724 USA (e-mail: nbergano@tycotelecom.com).

Digital Object Identifier 10.1109/JLT.2005.858255

## II. Undersea-Cable Systems

Fig. 2 shows an artist's concept of an undersea-cable transmission system joining two continents along with its major constituent parts (see, for example, [3]). The undersea-cable industry typically labels the equipment used under the water as "wet plant" and the terminal equipment used on land as "dry plant." The wet-plant equipment consists of the undersea cable, repeaters (i.e., amplification stages), and branching units. The typical intercontinental cable lengths are about 6000–7000 km to cross the Atlantic Ocean and about 9000–11 000 km to cross the Pacific Ocean. Thus, 6000 km is the distance typically thought of as "transoceanic." For these systems, repeaters are placed every 50–90 km to compensate for the cable's attenuation. Definitely, there are many undersea cables shorter than 6000 km. Also important (but not covered in this work) are the "repeaterless" systems [4], where the undersea part is simply cable. Note that the term "repeater" originates from the days when an operator would literally repeat what was spoken by one person on a first phone line to another person on a second phone line. The term repeater was somehow adapted to include the RF amplification stages placed on a transmission cable and was maintained through several paradigm shifts in technology, including today's optical-amplifier-based repeaters.

The "dry plant" or land-based equipment consists of the subsystems that are needed to operate the undersea cable, and interface the cable to the terrestrial network. This includes the special transponders (or simply transmitters and receivers) that can convert the terrestrial-grade short-haul signals into a format that can propagate through the undersea line. For example, this could be a transponder that has a short-reach interface at the standard synchronous digital hierarchy (SDH) rate on the client side, and a chirped return-to-zero (RZ) format with proprietary FEC overhead on the line side. In addition to the transponders, the dry-plant equipment include any dispersion precompensation and/or postcompensation, optical-line monitoring and fault-location equipment, and undersea-line powering equipment.

### A. Rich History of Undersea Cables

Undersea-cable systems have been in use for 140 years. The first successful transatlantic telegraph cable connected North America to Europe and went into service in 1866: 34 years after Samuel Morse invented the telegraph. At that time, an

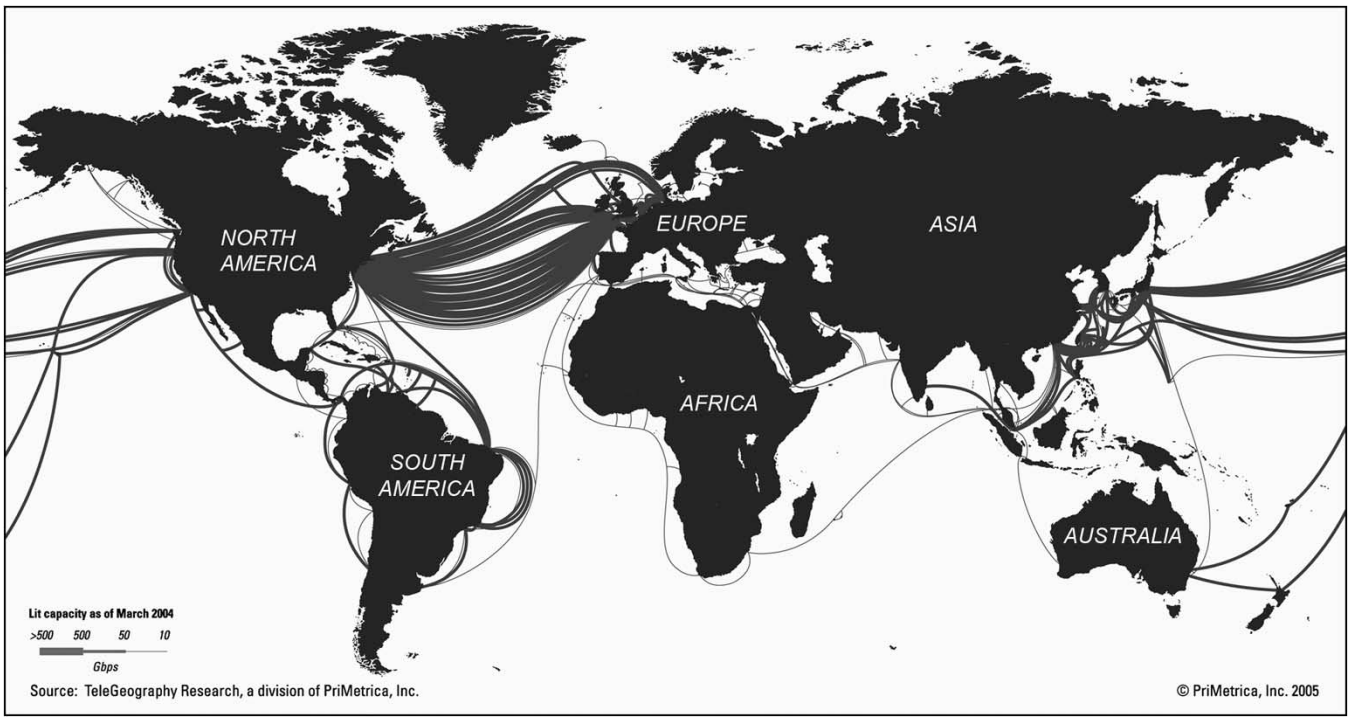


Fig. 1. World map showing the major undersea-cable systems that are in operation today. The thickness of the cable paths indicates the "Lit" capacity on each route. Source: TeleGeography Research, a division of PriMetrica, Inc.

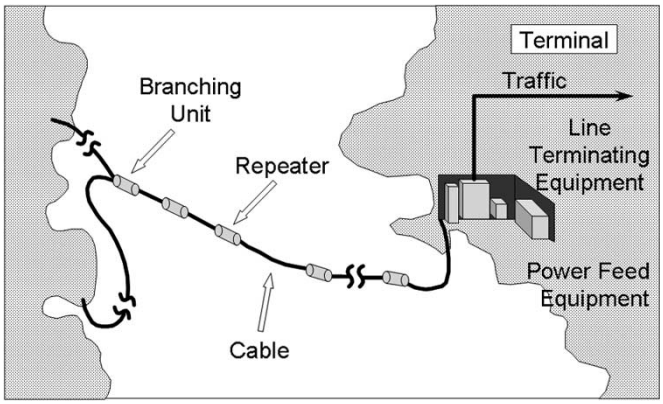


Fig. 2. High-level view of an undersea-cable communications system. The undersea portion contains cables and repeaters. The land portion contains equipment to power the undersea cable, undersea network-management equipment, and line-terminating equipment to convert the terrestrial-grade signal to a format that can go through the long undersea cable.

experienced telegraph operator could send about 17 words per minute at a cost of about $5 per word [5]. It took nearly 90 years from the time that the first telegraph cable was installed until the time when the first transatlantic telephone cable was installed. In 1956, the ***T***rans***A***tlantic ***T***elephone (TAT) cable system went into service with 36 4-kHz telephone circuits between Newfoundland and Scotland. These analog systems were based on coaxial cables with electronic amplifiers. Analog cable systems eventually grew in capacity to over 4200 voice circuits for systems installed as recently as 1983. These circuits were transmitted by frequency division multiplexing many circuits over an electrical bandwidth of a few tens of megahertz. The signals were boosted in "wideband" electrical amplifiers that were placed in repeaters and spaced approximately every 10 km. In an interesting twist of fate, the cable in the coaxial systems was linear, while great design efforts were expended to cope with the nonlinearity of the electronic amplifiers, which is opposite from the present optically amplified fiber-optic systems.

Early in the 1980s, work began in earnest to develop the first-generation fiber-optic undersea-cable system [6]. The transformation of the undersea-cable industry from RF coaxial to digital regenerator systems was of course a major undertaking that required many years of studies on both the component and system levels. Many research groups worked on important system-level issues such as jitter accumulation [7], mode partition noise [8], [9], dispersion penalty, and the need for an impairment budgeting process that could account for aging and repair margins. This technology change resulted in a significant increase in end-to-end capacity and repeater spacing.

Fig. 3 shows the cumulative full capacity of transatlantic cables installed over the past five decades. What is truly remarkable is that total transmission capacity has increased by $10^4$ since the time of the last analog coaxial system. The majority of this increase resulted from optical-amplifier technology.

Research on optical-amplifier-based transmission systems started late in the 1980s. At the time, it was not obvious that a high-speed optical signal could be transmitted over many thousands of kilometers without any intermediate regeneration. Also, a proof of concept was needed to show that the 1200 dB of optical gain needed to compensate the attenuation in 6000 km of cable could be made stable and with sufficient optical bandwidth to support gigabit operation. Many of these issues were

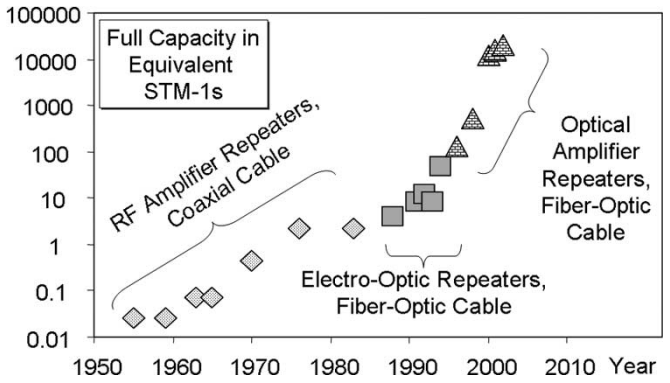


Fig. 3. Full capacity of transatlantic cable systems installed over the past five decades, displayed in STM-1's (or "equivalent STM-1s" for the analog systems).

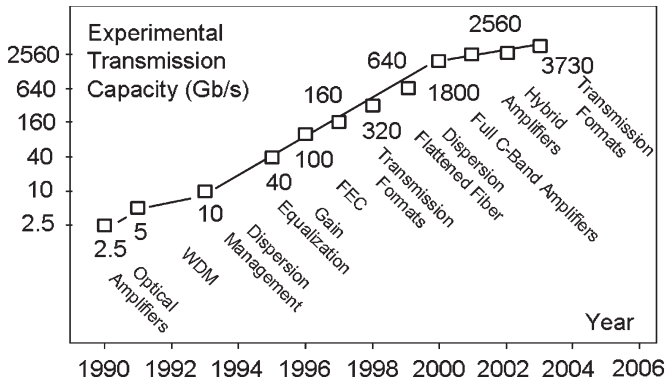


Fig. 4. Capacity of transoceanic-length transmission experiments measured in Gb/s, and the associated technology milestones. During the 1990s, the demonstrated capacity rapidly increased as more and more optical bandwidth was used. The rate of increase slowed dramatically in the early 2000s when the full EDFA bandwidth was exploited.

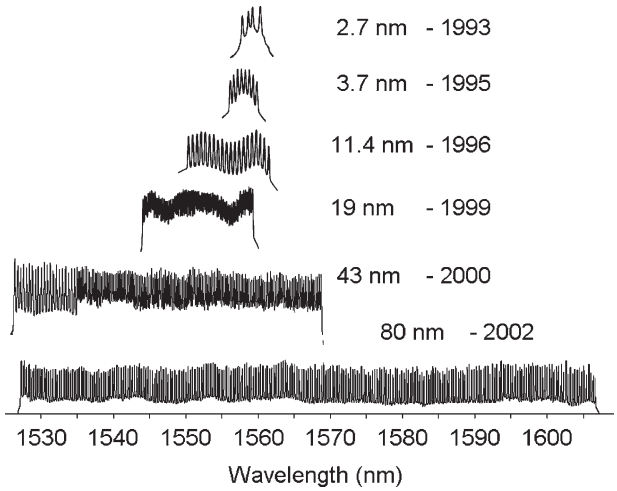


Fig. 5. Received optical spectrum of various WDM transmission experiments over the past 12 years. In each of the six curves, the amount of bandwidth is displayed along with the year that the work was published. The 43-nm result in the year 2000 corresponds to the full EDFA C-band. The 80-nm result in the year 2002 corresponds to the EDFA's C- and L-bands.

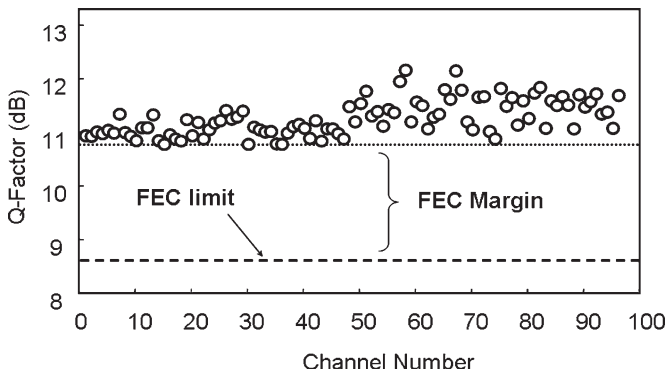


Fig. 6. Measured $Q$-factor versus channel number after the 9000-km transmission for the 96-channel operation on the TGN Pacific system. The lower dashed horizontal line labeled "FEC limit" is the $Q$-factor corresponding to error-free operation [12].

resolved by early transmission experiments using circulating loops [10] and straight-line testbeds [11]. Once the undersea-cable industry transitioned to single-channel optical-amplifier systems, research efforts focused on increasing capacity and reducing circuit cost by using WDM techniques.

Fig. 4 expands on the previous figure for the optical-amplifier era by showing the capacity of long-haul-system experiments and the technology milestones that were used. Over the 15-year period covered in the figure, the transmission capacity demonstrated for transoceanic lengths increased by more than 1000 fold! Many of the important technology milestones such as dispersion management, gain equalization, and new transmission formats were demonstrated. Fig. 5 shows the evolution of optical-bandwidth utilization of transoceanic experiments. The path to greater capacity in the WDM era was to increase the number of channels by using more optical bandwidth, by increasing the bit rate per channel, and by increasing spectral efficiency (i.e., putting the channels closer together). The change in slope of the curve in Fig. 4 around year 2000 corresponds to the time when the entire C-band was filled. Even though the total optical bandwidth eventually doubled with the use of both the C- and L-bands, the rate of capacity growth slowed once the C-band was filled.

### *B. State-of-the-Art Systems*

Today's modern undersea transmission systems are capable of terabit capacity, which was exclusively the realm of laboratory experiments just a few years ago. One of the most technologically advanced installed systems is the Tata Global Network (TGN) Pacific, which has connectivity between North America and Asia. This network has two Pacific crossings between Japan and Oregon (USA): undersea cables to Guam and California, and a number of terrestrial links. Each of the undersea-cable sections of TGN Pacific has eight fiber pairs. These cable sections were designed with a maximum capacity of 96 10-Gb/s optical channels per fiber pair.

Of particular interest is the $\sim$ 9000-km cable section installed between Hillsboro, OR, and Toyohashi, Japan. This segment uses many of the techniques listed in Fig. 4, including the newest dispersion-flattened fibers. Field tests confirmed that the segment could support the system-design capacity: 96 10-Gb/s customer channels per fiber pair [12]. Fig. 6 shows the $Q$-factors for a 96-channel operation, along with the FEC limit to obtain $< 10^{-15}$ bit error rate (BER) in the customer

TABLE I
SYSTEM PARAMETERS USED IN THE DESIGN EXAMPLE GIVEN IN SECTION III-G

| Parameter | Value | |
|---|---|---|
| System Length | 6,000 | km |
| Channel Count | 32 | |
| Repeater Spacing | 80 | km |
| Repeater Count | 75 | |
| Total Launch Power | 11.8 | dBm |
| Amplifier Noise Figure | 5 | dB |
| Channel Spacing | 75 | GHz |
| Amplifier Bandwidth | 19 | nm |
| Fiber Attenuation | 0.2 | dB/km |
| Dispersion Period | 500 | km |
| Dispersion Slope | 0.075 | ps/km-nm$^2$ |
| Effective Area (DSF) | 55 | $\mu$m$^2$ |
| (SMF) | 80 | |
| Line Rate (23% FEC overhead) | 12.3 | Gb/s |
| FEC "Error Free" Limit | 8.5 | dB |
| Transmitter Extinction Ratio | 13 | dB |
| Receiver Optical Bandwidth | 33 | GHz |
| Receiver Electrical Bandwidth | 9.2 | GHz |
| Receiver Back-to-back Q-factor | 21 | dB |

traffic. The average $Q$-factor is 11.3 dB, thus providing a minimum FEC margin of 2.2 dB.

## III. TECHNOLOGY OF UNDERSEA-CABLE SYSTEMS

The remainder of this paper will focus on the technology used to make possible these state-of-the-art systems. The technology discussion will focus on techniques used to transmit data over long lengths of optically amplified cables. The technology discussion will start with a description of the amplified transmission line and then broaden to include the terminal equipment, measures of system performance, transmission experiments and next-generation technology. Throughout this work, references are made to an illustrative 6000-km transoceanic system designed for 32 $\times$ 10-Gb/s WDM channels. The design parameters of this 6000-km example are reviewed in Table I and will be used in the calculation of such parameters as signal-to-noise ratio (SNR), $Q$-factors, and launch powers throughout this text.

### A. Undersea Amplified Line

Today's undersea systems use erbium-doped fiber amplifiers (EDFAs) to compensate for the attenuation in the optical-fiber cable [13]. Thus, in its most simple form, the undersea amplified line is a concatenation of single-mode fibers and optical amplifiers (Fig. 7). Depending on the particular system, the spacing between these repeaters are in the range of 50–90 km apart.

The total output power of each EDFA is controlled by simple gain compression [14]. Here, gain compression means the decibel difference between the small signal gain and the actual gain at the operating point (Fig. 7). Note that unlike RF amplifiers, EDFAs can be operated deep into gain compression without any distortion of the high-speed signals being amplified [15]. Remarkably, this simple technique works even for transoceanic-system lengths. The optical gain needed to propagate a signal across a typical 6000-km transatlantic system is about (0.2 dB/km) $\times$ (6000 km), or about 1200 dB just to compensate the loss in the cable. The total output-power control happens automatically by purposely designing the small signal gain of the amplifier to be several decibels larger than is needed to compensate for the cable span attenuation (Fig. 7). This creates a stable operating point where the total power gain equals the total loss across the gain spectrum of the amplifier.

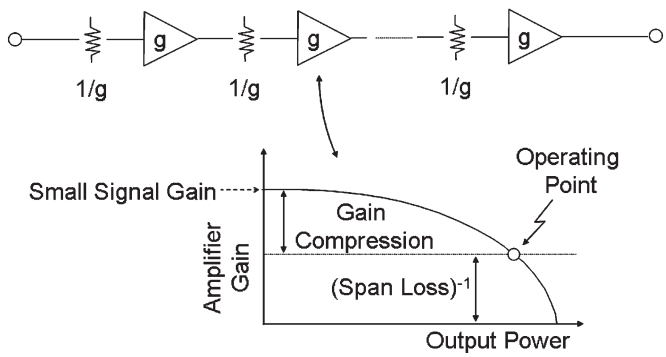


Fig. 7. Gain compression in the EDFA is used for power control on the amplifier chain. The small signal gain of each EDFA is designed to be larger than is needed to compensate the loss of the fiber span. This creates a stable operating point where EDFA gain equals the span's attenuation.

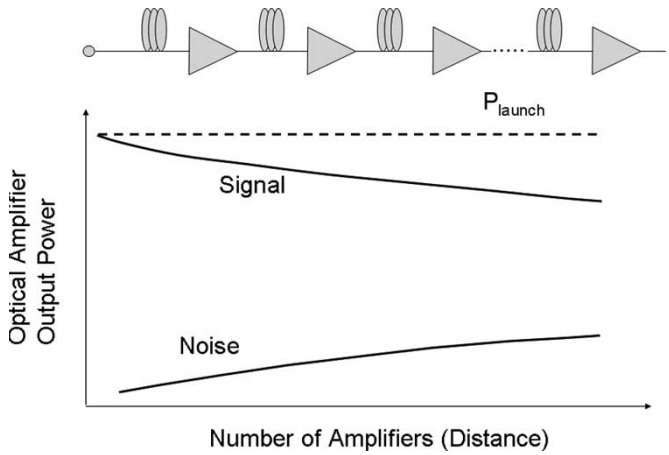


Fig. 8. Signal and noise propagation along a chain of optical amplifiers. The average signal level decreases along the amplifier chain since the noise generated in each amplifier accumulates, and the total output power of each amplifier is fixed by gain compression.

The noise generated in each EDFA and the noise that accumulates in the chain of amplifiers will limit the performance of a transmission system (see, e.g., [16]). Each amplifier in the chain generates a noise spectral density that can be approximated by[1]

$$\text{Noise Density} \approx h\nu(gNF - 1) \tag{1}$$

where $h\nu$ is the photo energy, $g$ is the EDFA external gain, and $NF$ is the amplifier noise figure (where $g$ and $NF$ are in linear units). This optical noise will accumulate along the amplifier chain and will ultimately dictate the spacing between amplifiers by limiting the received SNR. Noise accumulation also causes the level of the signal to decay, which is depicted in Fig. 8.

[1]Note that many variations on noise spectral density have been presented, which lead to slightly different approximations.

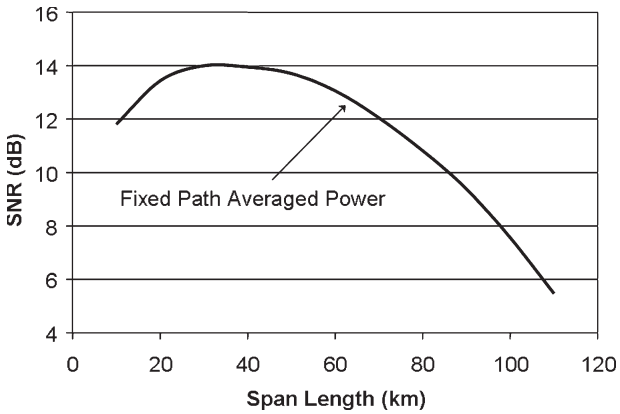


Fig. 9. Calculation of received SNR versus span length using (2) and (3). The input parameters are given in Table I. The calculation is performed for a fixed path-averaged power of 124 $\mu$W. This simplification ignores the signal decay shown in Fig. 8.

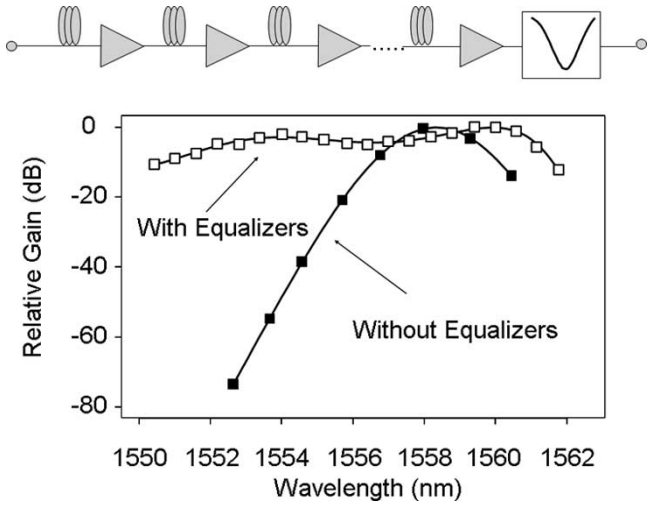


Fig. 10. Relative gain versus wavelength in a 6300-km amplifier chain. The optical bandwidth was expanded by about 3× using passive gain-equalizing filters.

This signal decay results from the total output power of the amplifiers being controlled by gain compression. The output power is made up of both signal and accumulated noise; thus, the signal level falls as the noise accumulates.

The SNR at the output of the amplifier chain can be approximated by

$$\mathrm{SNR_o} \approx \frac{P_{\mathrm{out}}}{NhvB_{\mathrm{o}}(gNF-1)} \tag{2}$$

where $P_{\mathrm{out}}$ is the individual channel's power out of the amplifier, $N$ is the number of amplifiers in the chain, and $B_{\mathrm{o}}$ is the optical bandwidth in which the SNR is expressed. The simplification given in (2) ignores the signal decay caused by noise accumulation. Fig. 9 shows this SNR, for the assumptions listed in Table I, as a function of repeater spacing calculated for a fixed path-averaged power [17]. The path-averaged power is a better metric for optical power from a system-design perspective, since the nonlinear impairments will be tied to the path-averaged power in a span, times the number of spans in the system. The relationship between the amplifiers's output power and the span's path-averaged power is given in (3) as

$$\begin{aligned}\overline{P} &= \frac{1}{L_{\mathrm{s}}}\int_0^{L_{\mathrm{s}}} P_{\mathrm{out}}10^{-\left(\frac{Al}{10}\right)}\mathrm{d}l \\ &= \frac{10P_{\mathrm{out}}}{AL_{\mathrm{s}}\ln(10)}\left(1-10^{-\left(\frac{AL_{\mathrm{s}}}{10}\right)}\right)\end{aligned} \tag{3}$$

where $L_{\mathrm{s}}$ is the span length, and $A$ is the fiber attenuation in decibels per kilometer.

The curve in Fig. 9 shows that as the span length increases beyond 40 km, the SNR decreases. This decrease in SNR resulting from using "lumped amplifiers" has been pointed out in several references for analog coaxial systems and for optical systems [18], [19]. This characteristic gives rise to the engineering tradeoff that shorter spans yield higher SNRs versus longer spans that yield fewer amplifiers (and lower cost). In a real system design, the span length is increased until the end-of-life margin matches the system's specification, which typically is in the range of 50–90 km for transoceanic-length systems.

WDM systems require the use of gain-equalization filters to expand and/or flatten the intrinsic gain shape of the amplifier chain. These filters can either be placed once after every $N$th amplifier (block equalization) and/or could be located at each amplifier. Block equalization (depicted in Fig. 10) is most useful in short systems, or where only a moderate amount of equalized optical bandwidth is required. Long-haul wideband systems usually require a combination of individual amplifier equalization and block equalization to achieve a usable bandwidth that is a large fraction of the EDFA's intrinsic bandwidth. For the design example given in Section III-G, each amplifier has its own gain-equalizing filter.

The end-to-end gain change over the optical bandwidth of the transmission line should be limited to about 5–10 dB for adequate performance. If a 10-dB gain error was equally distributed across a 6000-km system (75 amplifiers spaced 80 km apart), then the gain equalization needs to be accurate to within $\sim$ 0.1 dB per amplifier stage. While it might appear small, this level of gain equalization is routinely achieved for installed systems with optical bandwidths of about 28 nm. For example, Fig. 11 shows the optical spectrum before and after transmission through a 9000-km undersea cable installed in the Pacific Ocean [12]. As seen in the top of the figure, some pre-emphasis [20] was used in the transmitter to equalize channel performance. With optimum preemphasis, the range of channel output powers was less than 4 dB after the 9000-km transmission, as seen in the bottom of the figure.

Spectral hole burning [21] in the EDFA further complicates the design of a gain-flattened amplifier chain. The saturated EDFA output power of each WDM channel depends on the power in the neighboring channels averaged over some characteristic spectral hole-burning bandwidth. Thus, an EDFA amplifier chain does not have a simple "fixed" gain spectrum; rather, the gain shape depends on the spectral content of the input signals. This characteristic is seen for the case of partial loading of a long amplifier chain [22] in Figs. 12 and 13.

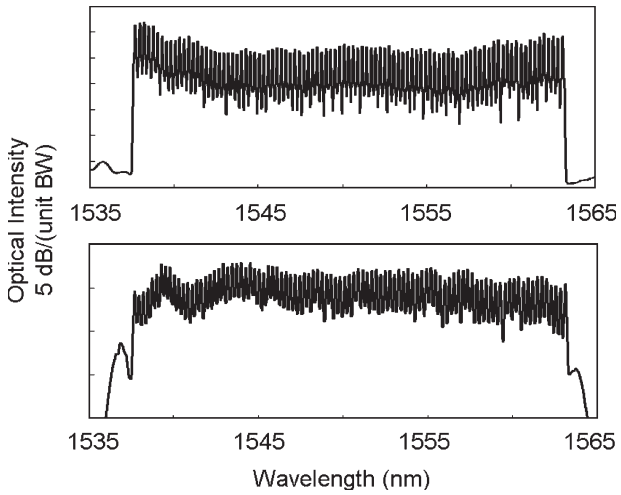


Fig. 11. Optical spectra from a field trial using 96 × 12.3 Gb/s per fiber over the first installed dispersion-flattened transpacific system, 9000-km long, part of the TGN. (Top) Input spectrum in Oregon, USA, and (bottom) output spectrum after the 9000-km transmission in Toyohashi, Japan, for the 96 channels at 12.3 Gb/s [12].

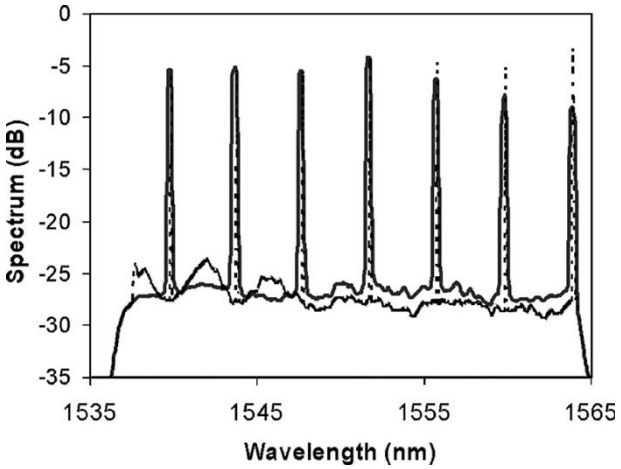


Fig. 12. Measured and simulated optical spectra for seven WDM signals uniformly spread across the passband of a 6650-km amplifier chain [22]. Note that the optical powers and SNRs for each channel are similar.

Here, a handful of channels are propagated through an amplifier chain with the channels spread across the entire band (Fig. 12) and with the channels concentrated in the center of the band (Fig. 13). Clearly, the gain of the middle channel in Fig. 13 is lower than in Fig. 12. A consequence of spectral hole burning is that the amplifier-chain gain shape is coupled to the input spectrum, which has advantages and disadvantages. On the plus side, spectral hole burning can help by reducing gain-equalization errors. On the negative side, spectral hole burning will limit the ability to adjust the output SNR with channel pre-emphasis.

### *B. Dispersion/Nonlinear Management*

The chromatic dispersion and the nonlinear index of the transmission fiber can reduce the performance of a WDM transmission system; thus, these characteristics must be considered in the system's design. Since the strength of optical nonlinearity

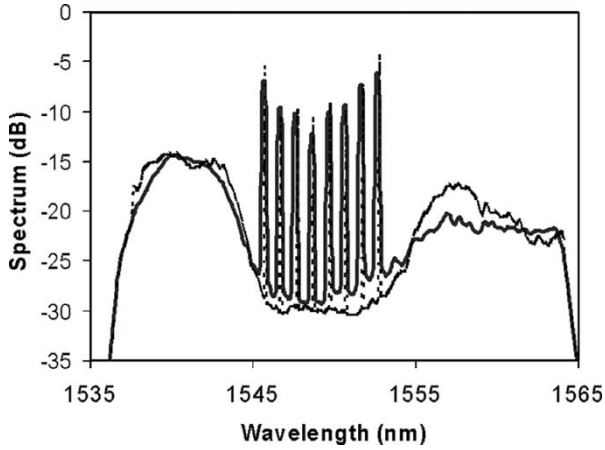


Fig. 13. Similar plot to that of Fig. 12 for the measured and simulated optical spectra of eight WDM channels after passing through a 6650-km-length system. In this case, the eight WDM channels were concentrated in the center of the passband. Note that the tightly spaced channels have depressed the gain for the center channel [22].

on a local level is quite small, the deleterious effects of the nonlinear index occur over many tens to hundreds of kilometers. This means that the nonlinear interaction lengths are long and that the local chromatic dispersion (which can be quite large) is an important factor in the system's performance. In fact, carefully tailoring the chromatic dispersion of the transmission line is the key to managing the nonlinear behavior of the system.

Chromatic dispersion can limit the maximum capacity and/or transmission distance of high-speed optical data channels. The dispersion-limited distance $(L_{\mathrm{D}})$ of a non-return-to-zero (NRZ) signal generated using an external modulator can be approximated by [23]

$$L_{\mathrm{D}} \approx \frac{6100}{B^2} \text{ km } (B \text{ in Gb/s}) \tag{4}$$

where it is assumed that the dispersion per unit length is about 17 ps/km·nm. For example, the dispersion-limited distance of a 10-Gb/s NRZ signal is about 60 km, or about 1000 ps/nm in terms of accumulated dispersion. Therefore, to transmit a 10-Gb/s signal (with low penalty), the accumulated dispersion needs to be lower than this 1000-ps/nm limit. In a purely linear sense, it does not matter how this dispersion accumulates, only the end-to-end value is important.

The central concept of dispersion management is that "local" dispersion will be used to reduce the nonlinear interactions between WDM signals, while the end-to-end dispersion is made small to ensure high signal quality [24]. Fig. 14 shows the four-wave mixing (FWM) efficiency between two optical channels through a fiber span with differing amounts of chromatic dispersion. Even though the nonlinear mixing process can be efficient for small channel spacing and dispersion, this mixing is dramatically reduced when the channels are far from the fiber's zero-dispersion wavelength.

Thus, for a high-performance long-haul system, it is desirable to have large local dispersion (to reduce nonlinear mixing) and low end-to-end dispersion (for high signal fidelity). These two characteristics are satisfied by using a "dispersion-managed" amplifier cable (also known as a "dispersion map")

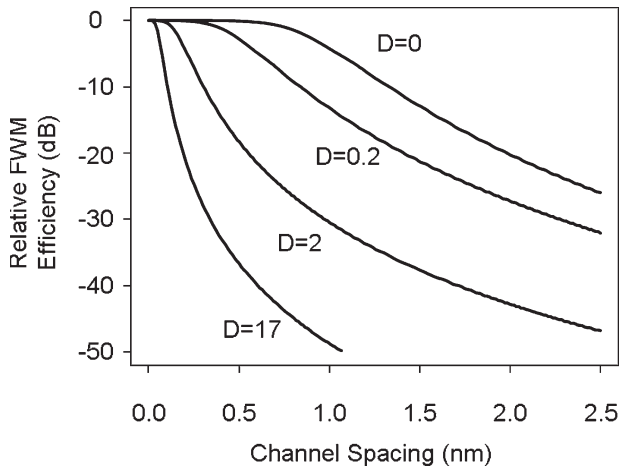


Fig. 14. Nonlinear mixing efficiency verses channel separation for two optical channels propagating through a single-mode optical fiber. The calculation is preformed for four different values of chromatic dispersion. The vertical axis was arbitrarily set to 0 for small channel spacing (following the model in [24]).

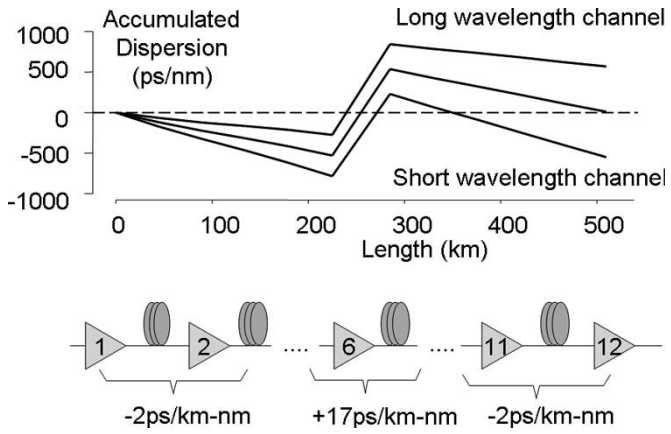


Fig. 15. Accumulated dispersion versus distance for the amplifier chain displayed in the bottom of the figure. The majority of the fiber in this dispersion map has an average dispersion of $-2$ ps/km $\cdot$ nm. This negative dispersion is compensated by using a conventional single-mode fiber that has an average dispersion of about $+17$ ps/km $\cdot$ nm.

[25]. In a dispersion-managed cable at least two different types of fiber are used with opposite signs of dispersion. Fig. 15 shows an example where sections of positive- and negative-dispersion fibers are concatenated so that the end-to-end accumulated dispersion is small, while maintaining a large local dispersion. In this example, the negative fiber has a mean dispersion of $-2$ ps/km $\cdot$ nm and the positive fiber has $+17$ ps/km $\cdot$ nm. The lengths of the two fiber types are selected to be in proportion to the ratio of dispersion values.

For the fiber arrangement in Fig. 15, the chromatic dispersion first accumulates negative dispersion, then positive, and eventually returns to 0 at the end of the dispersion period. The characteristic of returning to zero accumulated dispersion is only true for channels near the mean zero-dispersion wavelength. The higher wavelength channels accumulate positive dispersion and the lower wavelength channels accumulate negative dispersion. This characteristic is best understood by looking at the dispersion versus wavelength for each fiber type, as shown in the top of Fig. 16(a). This accumulated dispersion is a consequence of

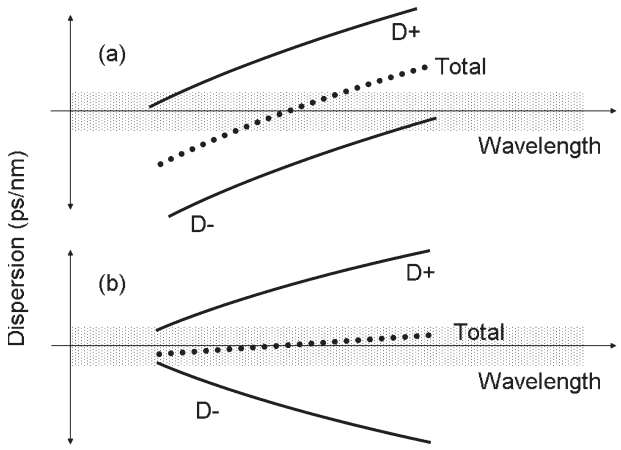


Fig. 16. Dispersion versus wavelength for (a) a conventional dispersion map and (b) a dispersion map using dispersion-flattened fiber.

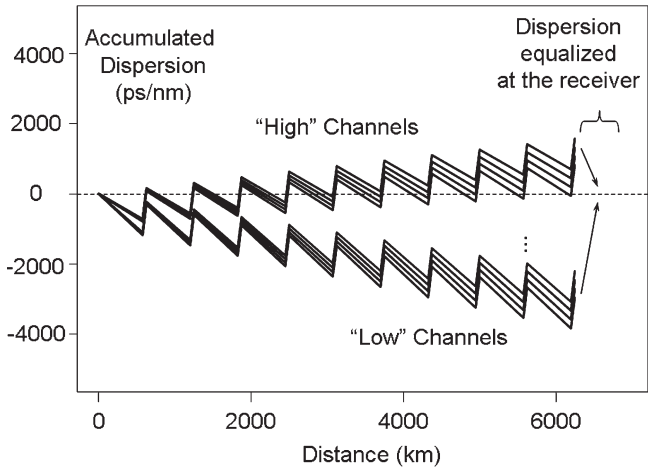


Fig. 17. Accumulated dispersion over an entire 6000-km transmission system that uses conventional non-slope-matched fibers.

both fiber types having a positive dispersion slope. Thus, the wavelength range over which the dispersion is compensated to a low value is limited to wavelengths near the mean zero-dispersion wavelength.

To obtain dispersion compensation over a wider range of wavelengths requires a different fiber type. Dispersion maps that have the widest compensation bandwidths use "dispersion-matched" or "dispersion-flattened" fiber [26]. In this dispersion map, the D- fiber is manufactured in such a way to make the dispersion-versus-wavelength characteristic "look" like the mirror image of the D+ fiber [27] so that the compensation bandwidth is much larger than with the conventional fiber [bottom of Fig. 16(b)] [28]. Stated more formally, the two fiber types are manufactured so that the relative dispersion slopes, or the ratio of the dispersion to the dispersion slope of the two fiber types, should be equal to obtain wide bandwidth compensation.

Fig. 17 shows a different view of this accumulated dispersion as a function of distance across 6000 km for several WDM channels for the dispersion map depicted in Fig. 15. The dispersion slope causes the accumulated dispersion in each channel to range over several thousand picoseconds per nanometer. This differential accumulated dispersion needs to be compensated at the terminals. This can be precompensation before the channels

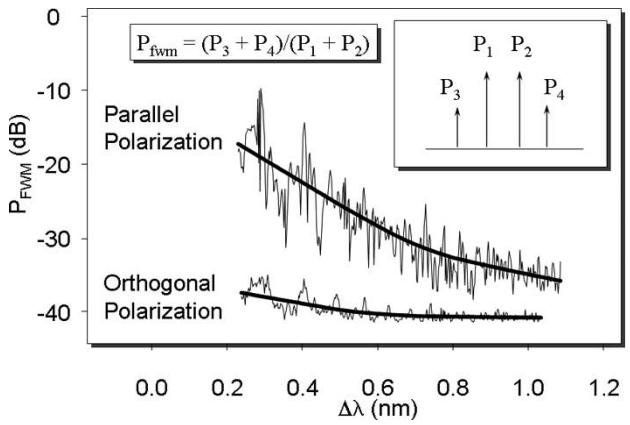


Fig. 18. Measured FWM efficiency versus channel separation in a 500-km amplifier chain. The upper wavelength channel is placed at the system's zero-dispersion wavelength. The upper curve is for parallel-polarization launch, and the lower line is for orthogonal-polarization launch.

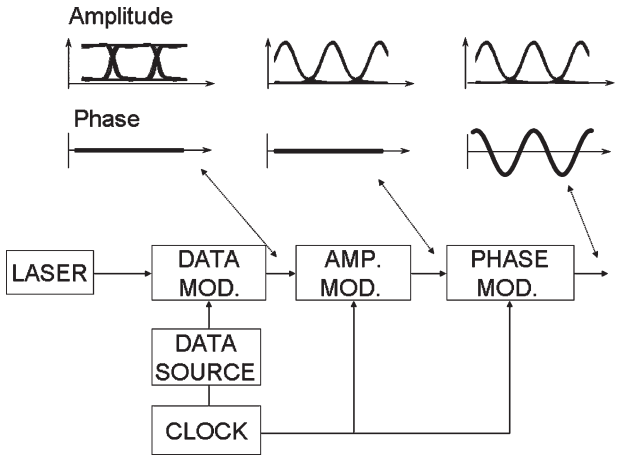


Fig. 19. Block diagram of a CRZ transmitter. Also shown are typical waveforms for the intensity and phase of the optical signal at intermediate points within the transmitter.

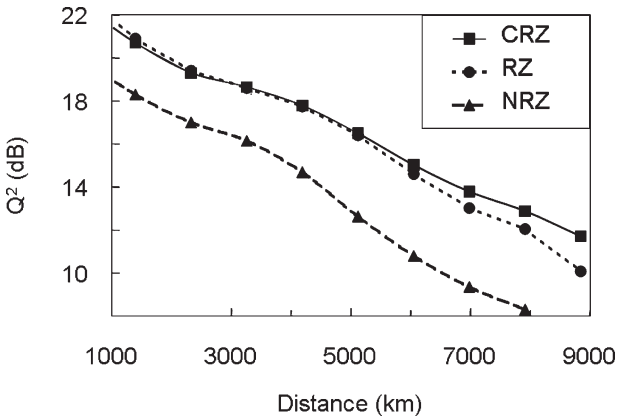


Fig. 20. $Q$-factor versus transmission distance for edge channel 2 of [38] with different modulation formats (CRZ with 1 rad phase modulation).

are multiplexed together at the transmit end, postcompensation after the channels are demultiplexed at the receiver, or a combination of both pre- and postcompensation [29].

Nonlinear interactions between WDM channels are polarization dependent (see, e.g., [30]). Understanding this polarization dependence will be important for the discussion on system design and margin allocation for $Q$-factor fluctuations. Fig. 18 shows an example of two-tone FWM through a 500-km amplifier chain [31] as a function of wavelength spacing for parallel and orthogonal polarizations [32]. When the two continuous-wave (CW) tones were launched in the same polarization, the two mix much more efficiently than when they were launched orthogonally polarized. Thus, one effective method of reducing the interactions between WDM channels is to launch the even-numbered channels orthogonally polarized with respect to the odd-numbered channels. This "pairwise" orthogonal method [33] greatly reduces nonlinear crosstalk from FWM and linear crosstalk such as nonideal extinction in demultiplexing devices, and has been used in many transmission experiments.

### C. Transmission Formats

Today, the subject of modulation formats is hot, but it is not new. Modulation formats have been debated over the entire history of optical-fiber communications. Early optical-fiber-transmission demonstrations used the NRZ modulation format because it was easy to generate and detect [34]. Many fiber-optic research organizations in the 1980s studied coherent optical-communication techniques [including differential phase-shift keying (DPSK)] to increase receiver sensitivity and selectivity [35]. Work on coherent optical communications slowed down dramatically in the early 1990s with the demonstration of the EDFA. Long EDFA-based systems started with the NRZ modulation format. Later, formats such as RZ and chirped RZ (CRZ) took hold for today's 10-Gb/s systems. Recently, there has been a strong interest in the DPSK format because of the 3-dB receiver advantage [36] and in bandwidth-reduced formats such as duobinary.

A robust transmission format that can propagate in the presence of dispersion, fiber nonlinearity, and accumulated noise is the chirped RZ pulse shape [37]. Fig. 19 shows a block diagram of a CRZ transmitter, and associated eye diagrams. CW laser light is modulated by an NRZ data stream at the required bit rate and is shaped by the bit-synchronous amplitude modulator. Prechirping is accomplished using a bit-synchronous phase modulator, with an adjustable peak-to-peak level and phase relative to the center of the bit. Mathematically, the complex amplitude of CRZ pulses is given by

$$A = \sqrt{P_{\text{peak}}} \cos\left(a\pi \sin(\pi F t)\right) \exp\left(ib \cos(2\pi F t)\right) \qquad (5)$$

where $P_{\text{peak}}$ is the "ones" peak power, $a$ is the level of amplitude modulation, $b$ is the phase-modulation index in radians, and $F$ is the bit rate. The typical pulsewidth at 100% amplitude-modulation level for a 10-Gb/s signal is 32 ps, and the peak power is 5.4 times higher than the time-average power.

The CRZ modulation format gives a performance advantage when a system is impaired by the transmission fiber's nonlinear index [38], [39]. Fig. 20 shows the $Q$-factor versus transmission distance measured in a circulating-loop experiment for RZ, NRZ, and for CRZ with a fixed phase-modulation index of 1 rad. Fig. 21 shows the $Q$-factor versus CRZ phase-modulation index at a fixed distance of 7900 km. When the transmission distance becomes long enough such that the fiber's nonlinear

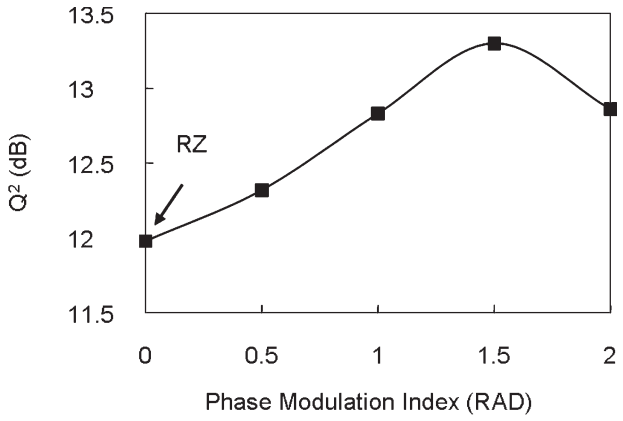


Fig. 21. $Q$-factor versus phase-modulation index for channel 2 [38] at 7900 km, employing CRZ.

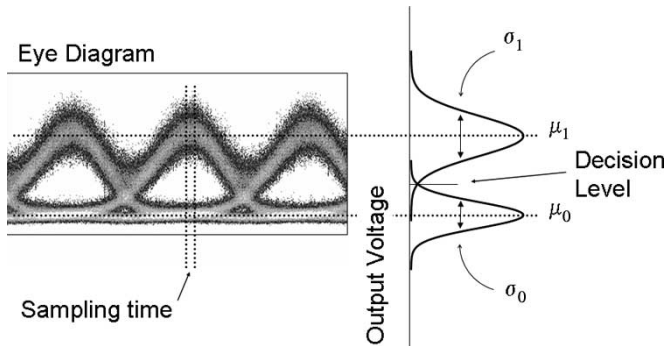


Fig. 22. Typical RZ eye diagram at the input to a decision circuit. The voltage samples that fall within the sampling window are used to form the histogram on the right-hand side. The upper and lower lobes of the voltage histogram have an associated mean and standard deviation.

behavior starts to limit the performance of the standard RZ format, the CRZ format has a performance advantage (at the expense of using more optical bandwidth).

A simplified explanation of this improvement can be given in either the time or the frequency domains. In the time-domain argument, the added bandwidth given by the phase modulation coupled with the fiber's dispersion spreads the data pulses over many bits, thus quickly changing the signal intensity and averaging nonlinear phase shift for different time samples of the signal. This fast intensity evolution of the signal with distance lowers not only self-phase-modulation effects in the same channel but nonlinear interaction between neighboring channels as well. In the frequency-domain argument, the phase modulation spreads the spectrum of the signal, thus reducing the peak amplitude of any particular Fourier component. These reduced spectral peaks lowers nonlinear mixing between spectral components of other data signals or noise components, thus improving nonlinear tolerance.

### *D. Measures of System Performance*

The performance of a digital transmission system is specified in terms of the $Q$-factor [40]. The $Q$-factor is an equivalent electrical SNR at the input to the receiver that dictates the received BER. This SNR is depicted in Fig. 22, which shows a typical eye diagram with a voltage histogram at the sampling point. The upper and lower lobes of the distribution have an associated mean and standard deviation that are used to define the $Q$-factor given in (6). The $Q$-factor describes the performance of the entire transmission path from the optical transmitter, through the optical path, and into the receiver. The $Q$-factor was adapted from Personick's work on calculating the performance of receivers in lightwave links [41]. The $Q$-factor has become the standard parameter used to account for the various impairments in the design process of optical-amplifier systems and is used in the "impairment budget" given in Table II for the 32 × 10-Gb/s WDM example.

$$q \equiv \left(\frac{|\mu_1 - \mu_0|}{\sigma_1 + \sigma_0}\right) \tag{6}$$

TABLE II
TYPICAL IMPAIRMENT BUDGET FOR THE 6000-km TRANSMISSION-SYSTEM EXAMPLE GIVEN IN TABLE I

| | | |
|---|---|---|
| **1** | "Noise-limited" Q | **15.0** |
| **2** | Propagation impairments | 1.6 |
| **3** | Terminal tolerances/impairments | 0.5 |
| **4** | Manufacturing and environmental | 1.0 |
| **5** | Q time variations | 1.0 |
| **6** | Line Q | 10.9 |
| **7** | Receiver back-to-back Q | 21.0 |
| **8** | Observed Q | 10.5 |
| **9** | Aging/repairs | 1.0 |
| **10** | End-of-Life Q | 9.5 |
| **11** | Required Q with FEC | 8.5 |
| **12** | End-of-Life Margin | 1.0 |

The $Q$-factor is related to the system's BER through the complementary error function $\mathrm{erfc}()$ given by

$$\mathrm{BER}(q) = \frac{1}{2}\mathrm{erfc}\left(\frac{q}{\sqrt{2}}\right) = \frac{1}{\sqrt{2\pi}}\int_q^\infty \mathrm{e}^{-\frac{\alpha^2}{2}}\mathrm{d}\alpha$$

$$\text{where } \mathrm{erfc}(x) = \frac{2}{\sqrt{\pi}}\int_x^\infty \mathrm{e}^{-\alpha^2}\mathrm{d}\alpha \tag{7}$$

or in terms of the more standard error function $\mathrm{erf}()$

$$\mathrm{BER}(q) = \frac{1}{2}\left[1 - \mathrm{erf}\left(\frac{q}{\sqrt{2}}\right)\right]$$

$$\text{where } \mathrm{erf}(x) = \frac{2}{\sqrt{\pi}}\int_0^x \mathrm{e}^{-\alpha^2}\mathrm{d}\alpha. \tag{8}$$

It is often useful to have numerical approximations to calculate BER from $Q$-factor [42] and $Q$-factor from BER. These approximations are given in (9) and (10).

$$\mathrm{BER} \approx \frac{\mathrm{e}^{-\frac{q^2}{2}}}{q\sqrt{2\pi}} - \frac{\mathrm{e}^{-\frac{q^2}{2}}}{q\sqrt{2\pi}(q^2+2)} + \frac{\mathrm{e}^{-\frac{q^2}{2}}}{q\sqrt{2\pi}(q^2+2)(q^2+4)} - \frac{5\mathrm{e}^{-\frac{q^2}{2}}}{q\sqrt{2\pi}(q^2+2)(q^2+4)(q^2+6)} + \cdots \tag{9}$$

Note that the first term in (9) is the typical approximation used in many publications. Equation (9) also includes the next few higher order terms that are needed for a more accurate estimation, which is important when calculating BERs for low $Q$-factors, which are now typical for experiments with strong FEC. For example, using only the first term of (9) gives $> 10\%$ error for $Q$-factors less than $\sim 9.5$ dB, whereas including all the terms gives an estimate better than $1\%$ down to a $Q$-factor of 3 dB.

Equation (10) gives an approximation for the reverse operation of estimating $Q$-factor from BER [43].

$$\text{Let } t = \sqrt{-2Ln(\text{BER})}$$
$$q \approx t - \left[\frac{2.515517 + 0.802853t + 0.010328t^2}{1 + 1.432788t + 0.189269t^2 + 0.001308t^3}\right]. \tag{10}$$

In (6)–(10), the $Q$-factor is expressed as a unitless ratio denoted by a lower case "$q$." Often, it is more convenient to express $Q$-factor in decibels as $20\text{Log}(q)$. The factor of 20 (or $10\text{Log}(q^2)$) is used to maintain consistency with the linear noise-accumulation model. For example, a 3-dB increase in the average launch power in all of the spans results in a 3-dB increase in $Q$-factor (assuming signal-spontaneous beat noise dominates, and ignoring signal decay and fiber nonlinearity).

There are several ways to experimentally estimate the $Q$-factor of an optical transmission system based on BER, eye diagrams, and/or optical SNR (OSNR). It is desirable to have an estimate of $Q$-factor based on a measurement of BER. One difficulty using BER is that often, the line side of a transmission system runs "error free." In this case, other methods are required, such as using the decision-circuit method of estimating $Q$-factor, as described in [40], and in International Telecommunication Union (ITU) publication O.201 [44]. The direct measurement of line-side BER is made easier in modern optical systems that have FEC-enhanced terminals, as will be discussed next.

### *E. Error Correcting Codes*

All modern long-haul optical-communications systems use some form of forward-error-correcting codes to improve the useable system margin [45]. FEC adds additional information (in real time) to the original information to be transmitted over a channel such that at the receiver, the combination of the original information and added information can correct errors in real time [46]. This results in an increased bit rate of the line side, which might be $7\%$ for the first generation G.709 FEC, or up to $25\%$ in more modern codes. Fig. 23 shows a simple block diagram of an optical terminal that uses FEC.

Fig. 24 shows a plot of the BER performance of the standard G.709 $7\%$ Reed-Solomon (RS) FEC in terms of input $Q$-factor. The amount of margin added by the FEC is dependent on the output BER and is shown graphically as the horizontal distance between the two curves labeled "uncoded" and $Q_{\text{Net}}$. Note that the curve labeled "uncoded" is simply a plot of (7) or (8), with the $x$-axis displayed in decibels. At an output BER of $10^{-15}$,

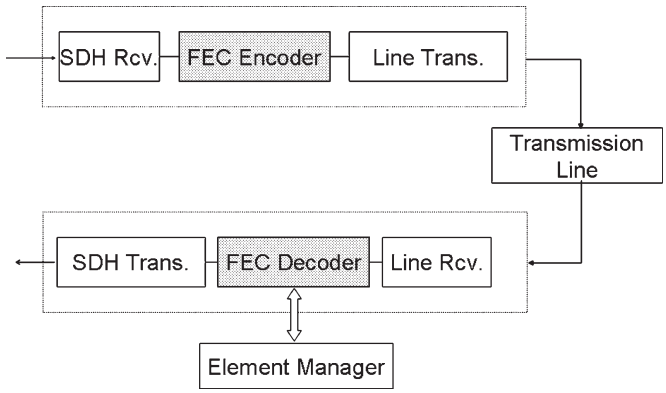


Fig. 23. FEC encoder and decoder are located between the client-side and line-side transponders. The actual bit rate transmitted on the line side is increased by the FEC overhead, which is typically between 7–25% for optical transmission systems.

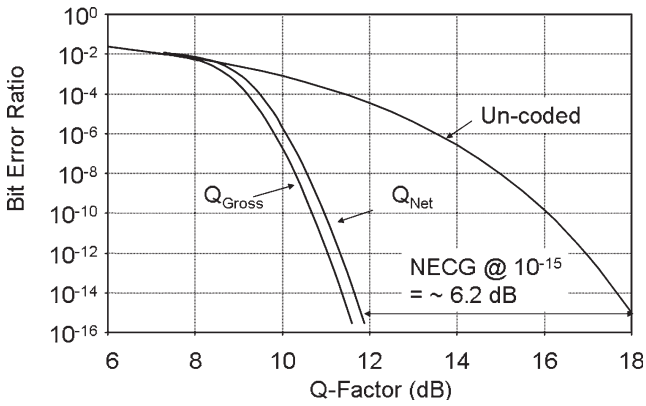


Fig. 24. Output BER versus input $Q$-factor. The top curve labeled "uncoded" is simply (7) or (8) plotted for input $Q$-factor expressed in decibels. The curve labeled $Q_{\text{Gross}}$ gives the input/output BER characteristics for the standard G.709 $7\%$ Reed-Solomon FEC algorithm. The curve labeled $Q_{\text{Net}}$ is shifted to the right by $\sim 0.28$ dB, which corrects for the added $7\%$ increase in bit rate.

the net effective coding gain for this FEC is about 6.2 dB. The horizontal shift between the curves labeled $Q_{\text{Net}}$ and $Q_{\text{Gross}}$ accounts for the change in bit rate when the overhead is added, or $10\text{Log}(1.067) \approx 0.28$ dB, where 1.067 is the ratio of bit rates before and after decoding.

The motivation for using FEC is to increase system margin, which, in turn, can be used to improve the performance of the system in several ways. For example, the FEC margin could be used for

1) increasing system capacity;
2) increasing system reach;
3) increasing the spacing between amplifiers;
4) decreasing system cost;
5) lowering the amplifier's output power (less pump power, fewer nonlinear impairments).

Another useful feature of FEC is the ability of the decoder to report an estimate of the error rate on the line side of the system. This is particularly important in order to know the channel's margin or $Q$-factor. For example, the link shown in Fig. 23 has an "element manager" or computer interface connected to the FEC decoder, which can report the line-side error ratio. Referring to the G.709 FEC example in Fig. 24, the decoder can

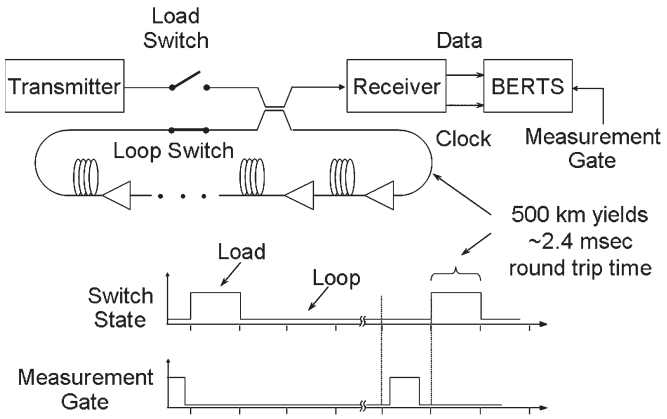


Fig. 25. Top: Block diagram for a circulating-loop experiment. Bottom: Timing diagram for a circulating-loop measurement showing the optical switch states and the time gate for making measurements.

directly measure the line BER in the range of $10^{-5}$ to $10^{-15}$, while the client side runs error free.

### *F. Transmission-Experiment Techniques*

Transmission experiments are an important part of the system-design process. This is especially true when new technologies and/or techniques are being introduced for the first time. For example, using EDFAs in undersea-cable systems is obvious today; however, in 1990, it was not obvious that an EDFA-based amplifier chain would work in a long cable system. Circulating-loop transmission experiments provided the first proof of concept that an amplifier chain based on EDFAs could be made stable and could support a high-speed optical channel over transoceanic distances [47]. Later, long amplifier chains were constructed to make full-length testbeds to demonstrate the feasibility of using EDFAs in optical transmission systems [11].

Most long-haul transmission experiments using optical amplifiers fall into one of three categories, including circulating loops, straight-line testbeds, and special measurements performed on installed systems [48]. Circulating-loop transmission measurements are, by far, the most important experimental technique. Circulating-loop techniques, applied to an amplifier chain of modest length, can provide an experimental platform to study a broad range of transmission phenomena for EDFA-based transmission systems.

A loop experiment attempts to simulate the transmission performance of a multithousand-kilometer-long system by making multiple passes through an amplifier chain of modest length (i.e., hundreds of kilometers). The loop transmission experiment (Fig. 25) contains most of the elements found in conventional experiments, such as an optical data transmitter/receiver pair, a chain of amplifier/fiber sections, and diagnostic equipment such as a BER test set (BERTS). In the loop experiment, optical switching is added to allow data to flow into the amplifier chain (the load state) and then to allow data to circulate (the loop state). The data circulates for a specified time, after which the state of the experiment toggles, and the load/loop cycle is repeated. The length of the amplifier chain used in the loop experiment is an engineering tradeoff between cost and performance. To perform meaningful experiments, many in the lightwave community have settled on a minimum amplifier chain of about 500 km.

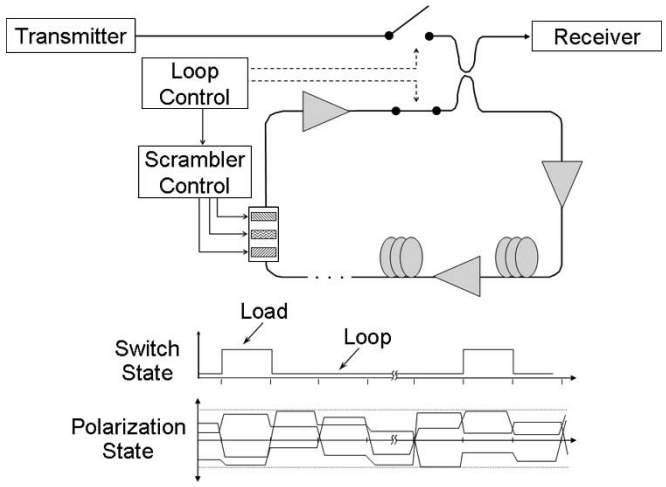


Fig. 26. Top: Block diagram of a circulating-loop experiment with a loop-synchronous polarization switching (modeled after [49]). Bottom: Simple timing diagram for the loop experiment along with typical drive signals for the polarization controller.

A new technique of using a loop-synchronous polarization switching has been recently demonstrated to give improved polarization emulation of straight-line transmission [49]. This new technique addresses one of the remaining disconnects between a loop and straight-line transmission experiment, namely, the accumulation of polarization-dependent loss and polarization mode dispersion [50]. Fig. 26 shows a multisection polarization controller within the loop, and a simplified timing diagram. The important characteristic of the drive signal is that the retarding angles within the polarization controller are held constant during the propagation of optical signals through the amplifier chain. Then, in between each subsequent "revolution" of the signal, the state of the polarization scrambler is randomized, and then held constant again.

The loop-synchronous polarization-control technique is particularly useful to improve the accuracy of $Q$-factor measurements in circulating-loop experiments. This technique is essential for shorter loops ($\ll$ 500 km) and for high-bit-rate experiments that are impaired by polarization mode dispersion. Using this technique, it is possible to measure accurately both the mean and fluctuation level of the $Q$-factor in a circulating-loop transmission experiment [51].

### *G. System-Design Example*

This section reviews a simplified design process for a 6000-km-length undersea-cable system, where the key design parameters are given in Table I. The target transmission capacity for this system is 32 10-Gb/s channels. An "impairment budget" will be used to account for the expected $Q$-factor performance [52]. The impairment budget will start with the ideal noise-limited performance and then account for all of the known impairments that are typically encountered in real systems. This process will arrive at an estimate of the expected end-of-life performance of the installed system, thus giving

an estimate of the operating margin. The design process goes as follows.

1) Determine the performance of the terminal equipment to obtain the minimum $Q$-factor at the receiver's input for error-free operation (after the FEC decoder).
2) Make an educated guess for the total margin above the terminal's FEC limit for "noise-limited" operation.
3) Design the amplifier chain over a range of repeater gains (i.e., span lengths).
4) Estimate output power and noise figure given a max pump power, channel spacing, and wavelength range.
5) Calculate the noise-limited performance and select a span length and output power.
6) Perform nonlinear signal-propagation modeling to estimate actual performance.
7) Populate the impairment budget with realistic margins.
8) Iterate to a solution.

As a starting point, it is assumed that the FEC performance gives an error-free point at an input $Q$-factor of about 8.5 dB, assuming a 23% overhead concatenated RS code [26]. Onto this 8.5-dB target, 6.5 dB is added as an initial guess for the total amount of margin needed over and above the FEC threshold, which gives a starting point of 15 dB mean $Q$-factor target. This 15-dB value appears in line 1 of the impairment budget given in Table II.

The next step is to arrive at an initial guess for the amplifier design to estimate the output power, mean gain, gain shape, and noise figure consistent with the 15-dB $Q$-factor target. Fig. 27 shows a typical amplifier block diagram and one particular gain shape, calculated for 16 dB of useable average gain, with $-3$ dBm average input power. The amplifier calculations were performed using the standard Giles model [53] with addition of spectral hole burning [22]. A gain-equalizing filter is designed with the inverse attenuation profile to the amplifier gain, yielding flat output-power characteristics over the 19 nm of required optical bandwidth. The total output loss of 2.7 dB can account for all excess losses in the gain-equalizing filter and output isolator. Amplifier designs are made for a range of usable gains and output powers consistent with the 15-dB $Q$-factor target.

$$q \approx \frac{2k\ \mathrm{SNR}\left(\frac{\mathrm{Er}-1}{\mathrm{Er}+1}\right)\sqrt{\frac{B_\mathrm{o}}{B_\mathrm{e}}}}{\sqrt{1+4k\ \mathrm{SNR}\left(\frac{\mathrm{Er}}{\mathrm{Er}+1}\right)}+\sqrt{1+4k\ \mathrm{SNR}\left(\frac{1}{\mathrm{Er}+1}\right)}}. \quad (11)$$

Equation (11) gives a $Q$-factor estimate in terms of OSNR for an RZ transmitter. Here, $Q$-factor and SNR are expressed as a linear ratio, $B_\mathrm{o}$ and $B_\mathrm{e}$ are the receiver's optical and electrical bandwidths, Er is the extinction ratio of the transmitter, and the parameter $k$ is typically 1.4 for the RZ format. The SNR in (11) could be calculated using the power level from (2), which is written in terms of output power from the amplifier delivered to the fiber span. Alternatively, optical powers could be expressed in terms of path-averaged (or length-averaged) power. The path-averaged power is a better metric for optical power from a system-design perspective, since the nonlinear impairments will be tied to the path-averaged power in a span, times the number of spans in the system. Thus, together, (2), (3), and (11) can be used to estimate the $Q$-factor from system parameters such as amplifier count, amplifier spacing, amplifier noise figure, and the optical power launched into the span. The results of this calculation are displayed in Fig. 28. The figure gives a curve of $Q$-factor versus span length for a fixed path-averaged power. This particular curve gave a span length of 80 km for the target $Q$-factor of 15 dB for a pump power of 80 mW into the erbium-doped fiber. Thus, the amplifier chain is designed with 80-km spans using a dispersion map similar to Fig. 17. The accumulated dispersion for the outer channels is compensated at the terminals.

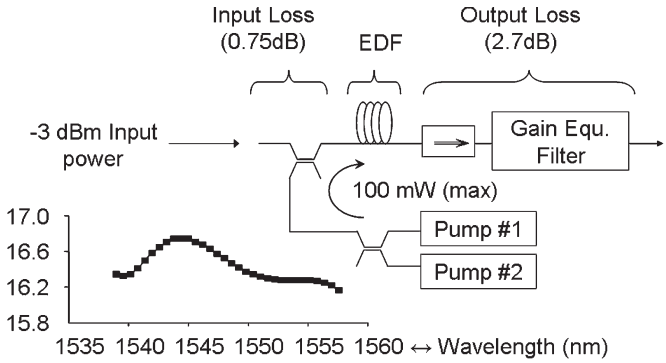


Fig. 27. Block diagram for an EDFA with redundant pump lasers. The average input attenuation is 0.75 dB and the average output attenuation is 2.7 dB. The curve at the bottom left shows the calculated gain assuming a flat output attenuation and an average input power of $-3$ dBm.

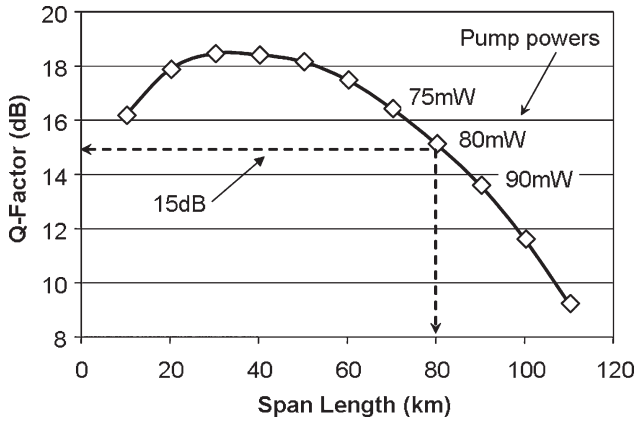


Fig. 28. Calculated $Q$-factor versus span length using (2), (3), and (11), and the values in Table I. These data were calculated for a fixed path-averaged power of 124 $\mu$W per channel.

At this point, there is enough information to start more detailed computer modeling of the transmission system to obtain more accurate estimates of transmission performance (which, unfortunately, is beyond the scope of this paper). For example, Golovchenko *et al.* [54] gave a detailed treatment how to model both the linear and nonlinear impairments found in long optical transmission systems. This comprehensive modeling includes amplifier gain shape (including spectral hole burning), signal decay caused by noise accumulation, chromatic dispersion, the fiber nonlinear index, Rayleigh scattering, and Raman crosstalk between channels. Using the parameters given in this example, the estimate of the transmission impairments is about 1.6 dB, which appears as line 2 of Table II. The interpretation of this value is that there is 1.6 dB of added penalty over and above the

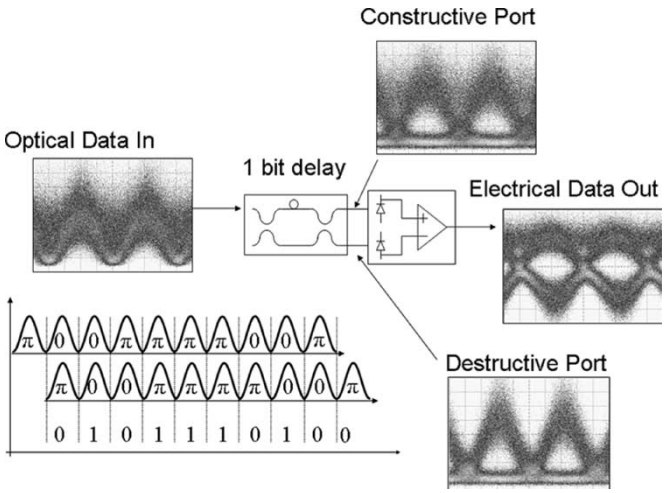


Fig. 29. Block diagram of a DPSK receiver, along with typical eye diagrams at intermediate points within the receiver. The eye diagrams were measured after 11 000 km [58].

performance predicted by the simple noise-accumulation theory of (2), (3), and (11).

Line 3 in the impairment budget allocates 0.5 dB for the terminal's implementation (i.e., transmitters and receivers), departing from the ideal performance. For example, the wavelengths can drift in the transmitter's laser and/or the receiver's filter and the decision point in the receiver can depart from the ideal. Line 4 in the impairment budget allocates 1.0 dB for the real manufacturing process, where statistical variations on the parts and the variability in the way the parts are assembled are considered.

Line 5 in the impairment budget allocates 1.0 dB for $Q$-factor variations. Standard telecommunications fibers do not maintain the state of polarization. Changes in the signal's polarization coupled with polarization dependence in the amplifier chain will cause the received BER to fluctuate with time [55]. Polarization drifts caused by temperature and/or pressure changes can be slow, or polarization changes caused by moving fibers in the terminal can be fast. Thus, line 5 accounts for these fluctuations by allotting 1 dB of margin for $Q$-factor fluctuations.

Line 6 (the difference between line 1 and the sum of lines 2–5) is the worst-case $Q$-factor that would be observed using a perfect receiver. Translating this to a $Q$-factor observed with a real receiver required the introduction of a new parameter, namely, the receiver "back-to-back" $Q$-factor. Equation (12) gives a simple relationship between the observed, line (or ideal), and the back-to-back $Q$-factors as

$$\frac{1}{q^2_{\text{Observed}}} = \frac{1}{q^2_{\text{bb}}} + \frac{1}{q^2_{\text{line}}} \tag{12}$$

where all the $Q$-factors are expressed as a linear ratio. Finally, an allotment of 1 dB is made for the system's aging and repair, which brings the expected end-of-life $Q$-factor to 9.5 dB (line 10). This end-of-life value measured against the FEC target of 8.5 dB gives an end-of-life margin of 1 dB.

At this point, the entire process could be iterated to drive the end-of-life margin to a lower number. For example, the noise-limited $Q$-factor could be lowered by reducing the path-averaged power in the transmission span. This, in turn, would lower the nonlinear penalty, thus changing the values in the design.

### *H. Future Trends*

In today's market where low "first cost" is important, it is essential to have a comprehensive understanding of long-haul optical propagation than ever before. In the next generation of systems, lower first cost will be achieved by improved equipment performance and by designing systems closer to the margin limits. This will require a comprehensive system-level understanding of signal generation and detection in the terminals and optical propagation in the wet-plant equipment. This improved understanding will be achieved by a mix of transmission experiments and computer simulations.

The next generation of undersea systems will benefit from innovations in the dry- and wet-plant equipment such as transponders with new modulation formats, more powerful FEC codes, and new fiber types. For example, many laboratory experiments have obtained impressive transmission results using the RZ-DPSK modulation format [56]. The allure of RZ-DPSK is the potential 3-dB reduction in required received OSNR for a particular BER, which results from the demodulation and detection process [57]. Fig. 29 shows a block diagram of a DPSK receiver, along with measured eye diagrams after long-distance propagation. The advantage of DPSK is evident by comparing the optical input eye diagram at the left of Fig. 29 to the electrical eye diagram at the receiver's output. Notice the large noise level at the center of the optical eye, and the relatively "clean" electrical eye diagram at the output.

Two years ago, Cai *et al.* reported the successful transmission of 373 10-Gb/s RZ-DPSK channels (25-GHz spaced) over 11 000 km with 40% spectral efficiency [58]. In this experiment, 80 nm of continuous optical bandwidth was achieved by using a combination of EDFAs and Raman gain along with dispersion-flattened fiber transmission spans [59]. These experimental results used a "second-generation" FEC code with a $Q$-factor threshold (at $10^{-15}$ BER) of 8.6 dB at a line bit rate of 12.3 Gb/s. This FEC code is still a few decibels away from the Shannon limit; thus, significant FEC improvements are still possible. Efforts are underway to improve the net effective coding gain of FEC circuits using both hard- and soft-decision front ends. For example, Mitsubishi has reported the results for a soft-decision front-end turbo block code FEC [60], where the $Q$-factor threshold was reduced to 6.3 dB for $\sim 10^{-15}$ BER. Thus, it might be possible to obtain an additional 2 dB of coding gain with new FEC algorithms for next-generation transponders.

Improvements in the cable's single-mode fiber will give greater system performance. The next generation of dispersion-flattened fiber spans should have better dispersion, nonlinear-penalty, splice-loss, and attenuation properties. Even a relatively small improvement in span attenuation could give a significant system-margin advantage. For example, a next-generation 7000-km system could have repeater spacing of 100 km or more. Even a modest 0.01-dB/km attenuation improvement would reduce the span loss by a full decibel, which could translate into a more useable system margin.

In the future, Raman amplification might find more applications in undersea systems (see, e.g., [61]). Today, Raman amplification is being used in a limited roll to extend the reach of the longest repeaterless links. Going forward, Raman amplification could be used to either augment and/or replace the EDFA gain. For example, Ma *et al.* demonstrated a 240-km "repeater" spacing for a 5280-km transmission distance by using a combination of conventional EDFAs, remote EDFAs, and Raman amplification [62]. In another demonstration, Nissov *et al.* demonstrated a system where the majority of the optical gain was provided by distributed Raman gain [63]. The noise performance of the Raman amplifier chain was about 2 dB better than a similar amplifier chain using EDFAs. What is observed from the most recent long-haul Raman-amplification demonstrations is the subtle coupling between optimizing gain and the dispersion map when designing Raman spans [64].

## IV. Conclusion

The technology used in undersea transmission systems has steadily progressed, even though the current demand for new cable systems has been low. New state-of-the-art transoceanic systems have terabit per second maximum capacity, while being flexible enough to have an initial deployed capacity at a fraction of the maximum. Next-generation systems and future upgrades of existing systems will benefit from concepts emerging from system research such as new transmission formats and new forward error correction (FEC) algorithms.

## Acknowledgment

Clearly, the subjects reviewed in this paper are not the work of one individual; rather, it is a collective knowledge gathered by many organizations working over many years! The author expresses his deepest thanks to the team at Tyco Telecommunications for all of the years of hard work that went into developing the technology reviewed in this work.

## References

[1] N. S. Bergano, "Undersea fiber optic cable systems: High-tech telecommunications tempered by a century of ocean cable experience," *Opt. Photon. News Mag.*, vol. 11, no. 3, pp. 21–25, Mar. 2000.

[2] P. R. Trischitta and W. C. Marra, "Global undersea communications networks," *IEEE Commun. Mag.*, vol. 34, no. 2, p. 201, Feb. 1996.

[3] R. F. Gleason, C. D. Anderson, G. M. Bubel, A. A. Cabrera, R. L. Lynch, B. O. Rein, W. F. Sirocky, and M. D. Tremblay, "Submarine cable systems," in *The Encyclopedia of Telecommunications*, vol. 15, F. E. Froehlich, Ed. New York: Marcel Dekker, 1990.

[4] E. Brandon, "Unrepeatered systems—When to switch to a different technology," presented at the Submarine Optical Communications Conf. (SubOptic), Monaco, Mar. 2004, Paper TuB1.3.

[5] B. Dibner, *The Atlantic Cable*. Norwalk, CT: Burndy Library, 1959.

[6] P. K. Runge and P. R. Trischitta, "The SL undersea lightwave system," in *Undersea Lightwave Communications*, P. K. Runge and P. R. Trischitta, Eds. Piscataway, NJ: IEEE, 1986, ch. 4.

[7] P. R. Trischitta and E. L. Varma, *Jitter in Digital Transmission Systems*. Norwood, MA: Artech House, 1989.

[8] Y. Okano, K. Nakagawa, and T. Ito, "Laser mode partition noise evaluation for optical fiber transmission," *IEEE Trans. Commun.* vol. COMM-28, no. 2, pp. 238–243, Feb. 1980.

[9] K. Ogawa and R. S. Vodhanel, "Measurements of mode partition noise of laser diodes," *IEEE J. Quantum Electron.*, vol. QE-18, no. 7, pp. 1090–1093, Jul. 1982.

[10] N. S. Bergano and C. R. Davidson, "Circulating loop transmission experiments for the study of long-haul transmission systems using erbium-doped fiber-amplifiers," *J. Lightw. Technol.*, vol. 13, no. 5, p. 879, May 1995.

[11] H. Taga, N. Edagawa, H. Tanaka, M. Suzuki, S. Yamamoto, H. Wakabayashi, N. Bergano, C. Davidson, G. Homsey, D. Kalmus, P. Trischitta, D. Gray, and R. Maybach, "10 Gb/s, 9000 km IM-DD transmission experiments using 274 Er-doped fiber amplifier repeaters," presented at the Optical Fiber Communication Conf. (OFC), San Jose, CA, Feb. 1993, Post-deadline Paper PD1.

[12] B. Bakhshi, M. Manna, G. Mohs, D. I. Kovsh, R. Lynch, M. Vaa, E. A. Golovchenko, W. W. Patterson, B. Anderson, P. Corbett, S. Jiang, M. Sanders, H. Li, G. T. Harvey, A. Lucero, and S. M. Abbott, "First dispersion-flattened transpacific undersea system: From design to terabit/s field trial," *J. Lightw. Technol.*, vol. 22, no. 1, pp. 233–241, Jan. 2004.

[13] T. Li, "The impact of optical amplifiers on long-distance lightwave telecommunications," *Proc. IEEE*, vol. 18, no. 11, p. 1568, Nov. 1993.

[14] N. Edagawa *et al.*, "904 km, 1.2 Gb/s non-regenerative optical transmission experiment using 12 Er-doped fiber amplifiers," in *Proc. 15th Eur. Conf. Optical Communication (ECOC)*, Gothenburg, Sweden, Sep. 1989, vol. 3, pp. 33–36, Paper PDA-8.

[15] E. Desurvire, C. R. Giles, and J. R. Simpson, "Gain saturation effects in high-speed, multi-channel erbium-doped fiber amplifiers at $\lambda = 1.53$ $\mu$m," *J. Lightw. Technol.*, vol. 7, no. 12, pp. 2095–2104, Dec. 1989.

[16] C. R. Giles and E. Desurvire, "Propagation of signal and noise in concatenated erbium-doped fiber optical amplifier," *J. Lightw. Technol.*, vol. 9, no. 2, pp. 147–154, Feb. 1991.

[17] F. Forghieri, R. W. Tkach, and A. R. Chraplyvy, "Fiber nonlinearities and their impact on transmission systems," in *Optical Fiber Telecommunications IIIA*, I. P. Kaminow and T. L. Koch, Eds. San Diego, CA: Academic, 1997, ch. 8.

[18] J. P. Gordon and L. F. Mollenauer, "Effects of fiber nonlinearities and amplifier spacing on ultra-long distance transmission," *J. Lightw. Technol.*, vol. 9, no. 2, pp. 170–173, Feb. 1991.

[19] E. Lichtman, "Optimal amplifier spacing in ultra-long lightwave systems," *Electron. Lett.*, vol. 29, no. 23, p. 2058, Nov. 1993.

[20] A. R. Chraplyvy, R. W. Tkach, K. C. Reichmann, P. D. Magill, and J. A. Nagel, "End-to-end equalization experiments in amplified WDM lightwave systems," *IEEE Photon. Technol. Lett.*, vol. 4, no. 4, p. 428, Apr. 1993.

[21] E. Desurvire, J. L. Zyskind, and J. R. Simpson, "Spectral gain hole-burning at 1.53 $\mu$m in erbium-doped fiber amplifiers," *IEEE Photon. Technol. Lett.*, vol. 2, no. 4, pp. 246–248, Apr. 1990.

[22] A. Pilipetskii, S. Abbott, D. Kovsh, M. Manna, E. Golovchenko, M. Nissov, W. Patterson, B. Bakshi, M. Vaa, and S. M. Abbott, "Spectral hole burning simulation and experimental verification in long-haul WDM systems," in *Proc. Optical Fiber Communication (OFC)*, Atlanta, GA, Mar. 2003, pp. 577–578, Paper ThW2.

[23] H. Gnauck and R. M. Jopson, "Dispersion compensation for optical fiber systems," in *Proc. Optical Fiber Telecommunications IIIA*. San Diego, CA: Academic, 1997, ch. 7.

[24] F. Forghieri, R. W. Tkach, and A. R. Chraplyvy, "Fiber nonlinearities and their impact on transmission systems," in *Optical Fiber Telecommunications IIIA*, I. P. Kaminow and T. L. Koch, Eds. San Diego, CA: Academic, 1997, ch. 8.

[25] A. R. Chraplyvy *et al.*, "8 $\times$ 10 Gb/s transmission through 280 km of dispersion-managed fiber," *IEEE Photon. Technol. Lett.*, vol. 5, no. 10, p. 1233, Oct. 1993.

[26] C. R. Davidson *et al.*, "1800 Gb/s transmission of one hundred and eighty 10 Gb/s WDM channels over 7000 km using the full EDFA C-band," in *Proc. Optical Fiber Communication (OFC)*, Baltimore, MD, Mar. 2000, pp. 242–244, Post-deadline Paper PD25.

[27] L. Gruner-Nielsen, T. Veng, S. N. Knudsen, C. C. Larson, and B. Edvold, "New dispersion compensating fibers for simultaneous compensation of dispersion and dispersion slope of non-zero dispersion shifted fibers in the C or L band," in *Proc. Optical Fiber Communication (OFC)*, Baltimore, MD, Mar. 2000, pp. 101–103, Paper TuG6.

[28] T. Tsukitani *et al.*, "Low-loss dispersion-flattened hybrid transmission lines consisting of low-nonlinearity pure silica core fibers and dispersion compensating fibers," *Electron. Lett.*, vol. 36, no. 1, pp. 64–66, Jan. 6, 2000.

[29] T. Naito, T. Terahara, T. Chikama, and M. Suyama, "Four 5-Gb/s WDM transmission over 4760-km straight-line using pre- and post-dispersion compensation and FWM cross talk reduction," in *Proc. Optical Fiber Communication (OFC)*, San Jose, CA, 1996, pp. 182–183, Paper WM3.

[30] G. P. Agrawal, *Nonlinear Fiber Optics*. New York: Academic, 1989.

[31] N. S. Bergano *et al.*, "320 Gb/s WDM transmission (64 $\times$ 5 Gb/s) over 7200 km using large mode fiber spans and chirped return-to-zero signals,"

presented at the Optical Fiber Communication Conf. (OFC), San Jose, CA, Feb. 1998, Paper PD12.
[32] E. A. Golovchenko, N. S. Bergano, and C. R. Davidson, "Four-wave mixing in multi-span dispersion-managed transmission links," *IEEE Photon. Technol. Lett.*, vol. 10, no. 10, pp. 1481–1483, Oct. 1998.
[33] N. S. Bergano and C. R. Davidson, "Method and apparatus for improving spectral efficiency in wavelength division multiplexed transmission systems," U. S. Patent 6 134 033, Oct. 17, 2000.
[34] P. W. Shumate *et al.*, "GaAlAs laser transmitter for lightwave transmission systems," *Bell Syst. Tech. J.*, vol. 57, no. 6, p. 1823, Jul./Aug. 1978.
[35] R. A. Linke and A. H. Gnauck, "High-capacity coherent lightwave systems," *J. Lightw. Technol.*, vol. LT-6, no. 11, pp. 1750–1769, Nov. 1988.
[36] A. Gnauck *et al.*, "2.5 Tb/s (64 × 42.7 Gb/s) transmission over 40 × 100 km NZDSF using RZ-DPSK format and all-Raman-amplified spans," presented at the Oprical Fiber Communication Conf. (OFC), Anaheim, CA, 2002, Paper PD-FC2.
[37] N. S. Bergano *et al.*, "320 Gb/s WDM transmission (64 × 5 Gb/s) over 7200 km using large mode fiber spans and chirped return-to-zero signals," presented at the Optical Fiber Communication Conf. (OFC), San Jose, CA, Feb. 1998, Paper PD12.
[38] B. Bakhshi, M. Vaa, E. A. Golovchenko, W. W. Patterson, R. L. Maybach, and N. S. Bergano, "Comparison of CRZ, RZ and NRZ modulation formats in a 64 × 12.3 Gb/s WDM transmission experiment over 9000 km," in *Optical Fiber Communication Conf. (OFC)*, Anaheim, CA, Mar. 2001, pp. WF4-1–WF4-3.
[39] E. Golovchenko, A. N. Pilipetskii, and N. S. Bergano, "Transmission properties of chirped return-to-zero pulses and nonlinear intersymbol interference in 10 Gb/s WDM transmission," in *Proc. Optical Fiber Communication (OFC)*, Baltimore, MD, Mar. 2000, pp. 38–40, Paper FC3-1.
[40] N. S. Bergano, F. W. Kerfoot, and C. R. Davidson, "Margin measurements in optical amplifier systems," *IEEE Photon. Technol. Lett.*, vol. 5, no. 3, pp. 304–306, Mar. 1993.
[41] S. D. Personick, "Receiver design for digital fiber optic communications systems," *Bell Syst. Tech. J.*, vol. 52, no. 6, pp. 843–874, Jul./Aug. 1973.
[42] *Handbook of Mathematical Functions With Formulas Graphs, and Mathematical Tables*, M. Abramowitz and I.A. Stegun, Eds. Washington, DC: U.S. Dept. Commerce, 1972, p. 932. (AMS55), Equation 26.2.13.
[43] *Handbook of Mathematical Functions With Formulas Graphs, and Mathematical Tables*, M. Abramowitz and I. A. Stegun, Eds. Washington, DC: U.S. Dept. Commerce, 1972, p. 933. (AMS55), Equation 26.2.23.
[44] "ITU-T Series O: Specifications of measuring equipment," *Q-Factor Test Equipment to Estimate the Transmission Performance of Optical Channels*. (AMS55), Equation 26.2.23.
[45] P. V. Kumar *et al.*, "Error—Control coding techniques and applications, *Optical Fiber Telecommunications IVA*, I. P. Kaminow and T. Li, Eds. San Diego, CA: Academic, 2002, ch. 17.
[46] F. W. Kerfoot, "Forward error correction for optical transmission systems," presented at the Optical Fiber Communication Conf. (OFC), Los Angeles, CA, Mar. 2004, Short Course SC212.
[47] N. S. Bergano, J. Aspell, C. R. Davidson, P. R. Trischitta, B. M. Nyman, and F. W. Kerfoot, "A 9000 km 5 Gb/s and 21 000 km 2.4 Gb/s feasibility demonstration of transoceanic EDFA systems using a circulating loop," presented at the Optical Fiber Communications Conf., San Diego, CA, Feb. 18–22, 1991, Paper PD-13.
[48] J. C. Feggeler *et al.*, "10 Gb/s WDM transmission measurements on an installed optical amplifier undersea cable system," *Electron. Lett.*, vol. 31, no. 19, p. 1676, Sep. 14, 1995.
[49] Q. Yu, L.-S. Yan, S. Lee, Y. Xie, and A. E. Willner, "Loop-synchronous polarization scrambling technique for simulating polarization effects using recirculating fiber loops," *J. Lightw. Technol.*, vol. 21, no. 7, p. 1593, Jul. 2003.
[50] S. Lee, Q. Yu, L.-S. Yan, Y. Xie, O. H. Adamczyk, and A. E. Willner, "A short recirculating fiber loop testbed with accurate reproduction of Maxwellian PMD statistics," in *Proc. Optical Fiber Communication (OFC)*, Anaheim, CA, Mar. 2001, pp. WT2-1–WT2-3.
[51] M. Nissov, J.-X. Cai, A. N. Pilipetskii, Y. Cai, C. R. Davidson, A. Lucero, and N. S. Bergano, "Q-factor fluctuations in long distance circulating loop transmission experiments," presented at the Optical Fiber Communication Conf. (OFC), Los Angeles, CA, Mar. 2004, Paper FM6.
[52] J. Schesser, S. M. Abbott, R. L. Easton, and M. S. Stix, "Design requirements for the current generation of undersea cable systems," *AT&T Tech. J.*, vol. 74, no. 1, p. 16, Jan./Feb. 1995.
[53] C. R. Giles and E. Desurvire, "Modeling erbium-doped fiber amplifiers," *J. Lightw. Technol.*, vol. 9, no. 2, pp. 271–283, Feb. 1991.
[54] E. A. Golovchenko, A. N. Pilipetskii, N. S. Bergano, C. R. Davidson, F. I. Khatri, R. M. Kimball, and V. J. Mazurczyk, "Modeling of transoceanic fiber-optic WDM communication systems," *IEEE J. Sel. Topics Quantum Electron.*, vol. 6, no. 2, pp. 337–347, Mar./Apr. 2000.
[55] S. Yamamoto, N. Edagawa, H. Taga, Y. Yoshida, and H. Wakabayashi, "Observation of BER degradation due to fading in long-distance optical amplifier system," *Electron. Lett.*, vol. 29, no. 2, pp. 209–210, Jan. 1993.
[56] W. A. Atia and R. Bondurant, "Demonstration of return-to-zero signaling in both OOK and DPSK formats to improve receiver sensitivity in an optically preamplified receiver," in *Proc. Lasers and Electro-Optics Society (LEOS) Annu. Meeting*, San Francisco, CA, Nov. 1999, pp. 226–227, Paper TuM3.
[57] A. H. Gnauck and P. J. Winzer, "Optical phase-shift-keyed transmission," *J. Lightw. Technol.*, vol. 23, no. 1, pp. 115–130, Jan. 2005.
[58] J. X. Cai *et al.*, "A DWDM demonstration of 3.73 Tb/s over 11 000 km using 373 RZ-DPSK channels at 10 Gb/s," presented at the Optical Fiber Communication Conf. (OFC), Atlanta, GA, Mar. 2003, Post-Deadline Paper PD22.
[59] D. Foursa *et al.*, "2.56 Tb/s (256 × 10 Gb/s) transmission over 11 000 km using hybrid Raman EDFAs with 80 nm of continuous bandwidth," presented at the Optical Fiber Communication Conf. (OFC), Anaheim, CA, 2002, Post-Deadline Paper PD FC3.
[60] T. Mizuochi *et al.*, "Experimental demonstration of net coding gain of 10.1 dB using 12.4 Gb/s block turbo code with 3-bit soft decision," in *Proc. Optical Fiber Communication Conf. (OFC)*, Atlanta, GA, Mar. 2003, pp. PD21–P1-3.
[61] H. Kidorf, M. Nissov, and D. Foursa, "Ultra-long-haul submarine and terrestrial application," in *Raman Amplifiers for Telecommunications 2,* M. Islam, Ed. New York: Springer-Verlag, 2004, ch. 17.
[62] M. Ma, H. Kidorf, K. Rottwitt, F. W. Kerfoot, and C. Davidson, "240-km repeater spacing in a 5280 km WDM system experiment using 8 × 2.5 Gb/s NRZ transmission," *IEEE Photon. Technol. Lett.*, vol. 10, no. 6, pp. 893–895, Jun. 1998.
[63] M. Nissov, C. R. Davidson, K. Rottwitt, R. Menges, P. C. Corbett, D. Innis, and N. S. Bergano, "100 Gb/s (10 × 10 Gb/s) WDM transmission over 7200 km using distributed Raman amplification," in *Proc. 11th Int. Conf. Integrated Optics and Optical Fibre Communications, and 23rd Eur. Conf. Optical Communications*, Edinburgh, U.K., Sep. 1997, pp. 9–12.
[64] G. Charlet *et al.*, "WDM transmission at 6 Tb/s capacity over transatlantic distance, using 42.7 Gb/s differential phase-shift keying without pulse carver," presented at the Optical Fiber Communication Conf. (OFC), Los Angeles, CA, 2004, Post-Deadline Paper PDP36.

**Neal S. Bergano** (S'80–M'88–SM'90–F'99) received the B.S. degree in electrical engineering from the Polytechnic Institute of New York, Brooklyn, in 1981 and the M.S. degree in electrical engineering and computer science from the Massachusetts Institute of Technology, Cambridge, in 1983.

The main focus of his career has been understanding how to improve the performance and how to expand the transmission capacity of long-haul lightwave systems, including the use of wavelength division multiplexing (WDM) in optical-amplifier-based systems. In 1981, he joined the technical staff of Bell Laboratories' undersea systems division. In 1992, he was named a Distinguished Member of the Technical Staff of AT&T Bell Laboratories. In 1996, he was promoted to an AT&T Technology Consultant and in 1997 to an AT&T Technology Leader. He is currently the Managing Director of System Research at Tyco Telecommunications, Eatontown, NJ. He holds 25 U.S. patents in the area of lightwave transmission systems.

Mr. Bergano is a Fellow of the Optical Society of America (OSA) and of AT&T. He is a Member of the IEEE Lasers & Electro-Optics Society (LEOS) and the IEEE Communications Society (COMSOC). He served as an elected Member of the Board of Governors for IEEE LEOS from 1999 to 2001. He served as the Technical Co-Chair for the 1997 Optical Communications (OFC) conference and as the General Co-Chair for the 1999 OFC/IOOC conference. He also served as the Chair of the OFC steering committee from 2000 to 2002. He is presently the Vice President of Conferences for the IEEE LEOS. He is the recipient of the 2002 John Tyndall Award, "For outstanding technical contributions to and technical leadership in the advancement of global undersea fiber-optic communication systems."